

We are IntechOpen, the world's leading publisher of Open Access books Built by scientists, for scientists

6,900

Open access books available

186,000

International authors and editors

200M

Downloads

Our authors are among the

154

Countries delivered to

TOP 1%

most cited scientists

12.2%

Contributors from top 500 universities



WEB OF SCIENCE™

Selection of our books indexed in the Book Citation Index
in Web of Science™ Core Collection (BKCI)

Interested in publishing with us?
Contact book.department@intechopen.com

Numbers displayed above are based on latest data collected.
For more information visit www.intechopen.com



Assessment of Hardness Based on Phase Diagrams

Jose David Villegas Cárdenas,
Victor Manuel López Hirata,
Carlos Camacho Olguin,
Maribel L. Saucedo Muñoz and
Antonio de Ita de la Torre

Additional information is available at the end of the chapter

<http://dx.doi.org/10.5772/64699>

Abstract

This chapter summarizes the methodology and development of a general equation, in order to obtain a series of equations to assess the hardness of different Al-Cu-Zn alloys, based on their chemical composition. This methodology produces an assessment of hardness with a maximal deviation of 5%, in as-cast, homogenized and quenching alloys, for both alloys created in laboratories like commercials. This method entails the generation of linear equations by a linear regression method, obtained from a zone of the phase diagram, when the composition is changed from linear to planar form. Therefore, if the chemical composition of samples varies, the percentage of each phase will also vary, causing a change in mechanical properties in a linear manner. If the heat treatments are the same for all samples, then the changes in mechanical properties are proportional for each of them, maintaining the linear relationship in mechanical properties in accordance with chemical composition. This methodology is applicable for any ternary alloy along with its equilibrium diagram.

Keywords: quenching, Gibbs free energy, phase diagrams, alloys

1. Introduction

The cost of any product is primarily limited by the cost of raw materials. This determines 50% of the total product cost and that is why it is necessary to try and create products using cheaper materials, but that still possess the same physical, chemical and mechanical properties.

This phenomenon took place in China when the country started to create very cheap products, made possible thanks to the development of new, cheaper materials with the same mechanical properties as older, more expensive materials.

Even if cheaper materials are available, it is still necessary to assess their mechanical properties in order to decide whether the resultant product will be suitable.

In addition, in order to assess the mechanical properties of materials, it is necessary to know their phases, and this need is addressed by the phase diagram. The next section describes this in more detail.

2. Phase Diagrams

Phase diagrams in metallic alloys are a development of the relationship between the Gibbs free energy of the different phases that exist in a metallic mix. A phase is defined as “a portion of the system whose properties and composition are homogeneous and which is physically distinct from other parts of the system” [1].

Gibbs free energy measures the stability of a system according to certain temperatures and pressures. This energy generates a curve on the graphic representation of energy vs atomic percentage, and when the system in question has different phases, then each phase will generate a curve (**Figure 1(a)-(e)**).

The Gibbs free energy is defined by the equation:

$$G = E + PV - TS \quad (1)$$

Where:

E = Internal energy of the system

P = Pressure

V = Volume

T = Temperature

S = Entropy

In the case of binary alloys, the equation of Gibbs free energy is:

$$\Delta G_{mix} = N_a z \varepsilon X_A X_B + RT(X_A \ln X_B + X_B \ln X_A) \quad (2)$$

Where:

N_a is Avogadro's number

Z is the number of bonds per atom

ε is the difference between the A-B bond energy and the average of the A-A and B-B bond energies.

Equation (3) explain this further:

$$\varepsilon = \varepsilon_{AB} - \frac{1}{2}(\varepsilon_{AA} + \varepsilon_{BB}) \quad (3)$$

This can be simplified a little if $N_a Z \varepsilon = \Omega$

The graphic of the binary alloy with respect to the Gibbs free energy at a constant pressure and temperature, is used to create the phase diagram. **Figure 1** represents the formation of a phase diagram by the Gibbs free energy.

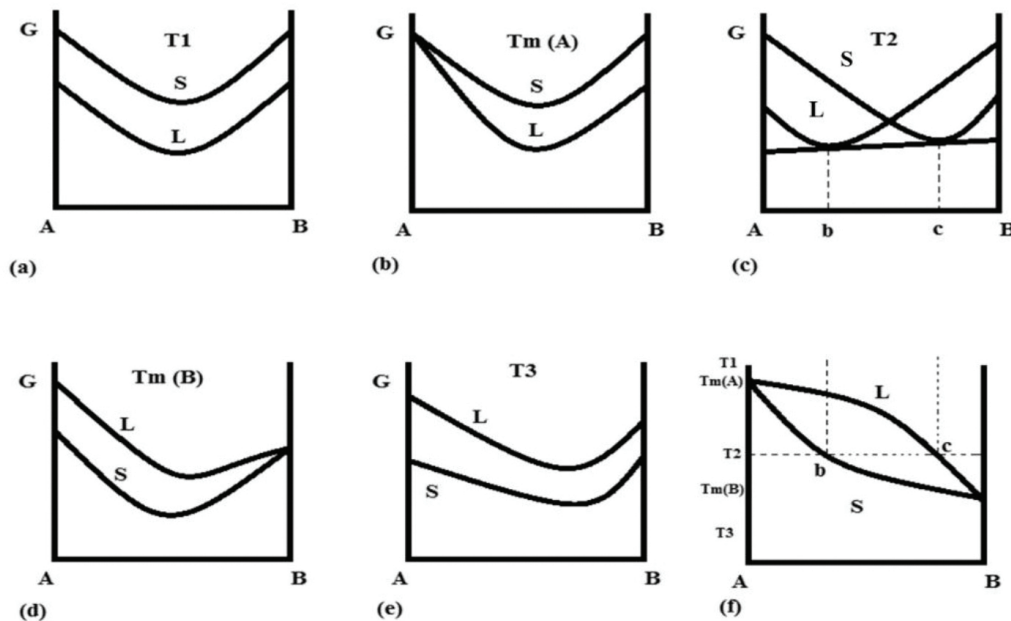


Figure 1. Phase diagram based on the Gibbs free energy in the liquid and solid phase.

Figure 1(a) shows both L and S phases, but in this case the L phase shows a lower energy in whole the combination percentage of the elements A and B. This indicates that the L phase is present in whole the combination of two elements at temperature T1, and this is shown in the phase diagram **Figure 1(f)**, where it can be observed that the temperature T1 is only observed the L phase in whole combination of elements A and B. If the curves generated is intercepted at a point in the temperature Tm, as is the case of **Figure 1(b)**, where an interception of the L and S phases can be observed. After this point, the L phase possesses less energy.

This is reflected in the phase diagram, where the temperature Tm (A) is observed in both phases at the initiation of the combination of A and B, and is later seen in the L phase only [2].

When the curves of Gibbs free energy intersect at certain temperatures, e.g. temperature T₂, then the phases are mixed. This mixing occurs in the tangent line between the curves of the L and S phases (**Figure 1(c)**). At the point where element A begins, to the point of interception with the tangent line, only the S phase is present. In the points where the curves are intercepted by the tangent line, a mix of L and S phases is obtained. Finally, from point c to the start of element B, only the L phase is present.

As **Figure 1** shows, at a certain temperature it is possible to have a mix of phases. This is important because the proportion of the phases determines the mechanical, physical and chemical properties of the metallic alloys.

In the previous investigations, equations were obtained that link hardness with chemical percentage – that is to say with the tangent line of the curves of Gibbs free energy. It is therefore necessary to understand the mathematical form in which the tangent line is obtained.

In order to better understand this, the example below shows the creation of a tangent line to two parabolas represented by the equations:

$$y = 2x^2 + x \quad (4)$$

$$y = 3x^2 + 2x \quad (5)$$

The curves generated by equations (4) and (5), and the tangent line are shown below in **Figure 2**:

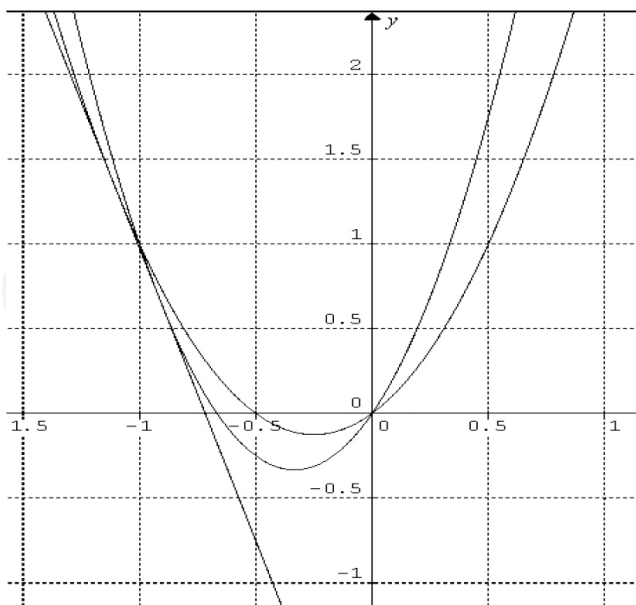


Figure 2. Graphic of equations (4) and (5) and associated tangent line.

The tangent line shown in **Figure 2** is represented by equation (6):

$$y = mx + b \quad (6)$$

However, at some points equation (6) is intercepted by equations (4) and (5) and then:

$$mx + b = 2x^2 + x \quad (7)$$

$$mx + b = 3x^2 + 2x \quad (8)$$

If we pass all of the left side of the equations, then:

$$2x^2 + x(1 - m) - b = 0 \quad (9)$$

$$3x^2 + x(2 - m) - b = 0 \quad (10)$$

The equation is solved using the quadratic equation:

$$x_{1,2} = \frac{-(1 - m) \mp \sqrt{(1 - m)^2 - 4(2)(-b)}}{2(2)} \quad (11)$$

$$x_{1,2} = \frac{-(2 - m) \mp \sqrt{(2 - m)^2 - 4(3)(-b)}}{2(3)} \quad (12)$$

However, equation (6) touch in only point to the equations (4) and (6), therefore when is applicate the quadratic equation the result into of square root.

$$(1 - m)^2 - 4(2)(-b) = 0 \quad (13)$$

$$(2 - m)^2 - 4(3)(-b) = 0 \quad (14)$$

By developing:

$$1 - 2m + m^2 + 8b = 0$$

$$4 - 4m + m^2 + 12b = 0$$

Then the quadratic equation is used:

$$m_{1,2} = \frac{2 \mp \sqrt{(-2)^2 - 4(1)(8b+1)}}{2(1)} \quad (15)$$

$$m_{1,2} = \frac{4 \mp \sqrt{(-4)^2 - 4(1)(12b+4)}}{2(1)} \quad (16)$$

As the slope is the same, it is possible to match equations (15) and (16).

$$\frac{2 \mp \sqrt{(-2)^2 - 4(1)(8b+1)}}{2(1)} = \frac{4 \mp \sqrt{(-4)^2 - 4(1)(12b+4)}}{2(1)}$$

$$2 + \sqrt{(-2)^2 - 4(1)(8b+1)} = 4 + \sqrt{(-4)^2 - 4(1)(12b+4)}$$

$$2 + \sqrt{4 - 32b - 4} = 4 + \sqrt{16 - 48b - 16}$$

$$2 + \sqrt{4 - 32b - 4} = 4 + \sqrt{16 - 48b - 16}$$

$$2 + \sqrt{-32b} = 4 + \sqrt{-48b}$$

Therefore, b is:

$$b = -\left[\frac{2}{\sqrt{32} - \sqrt{48}}\right]^2 = -2.4747$$

With this value, using equation (15) or (16) it is possible to obtain m:

$$2 + \sqrt{(-2)^2 - 4(1)(8(-2.4747+1))} = 4 + \sqrt{(-4)^2 - 4(1)(12(-2.4747+4))}$$

The equations are equal when $m = -3.4495$

The linear equation representing the tangent to each curve is:

$$y = -3.4495 \times -2.4747 \quad (17)$$

Using this method we can obtain the linear equation generated by the curves of Gibbs free energy in a regular solution. For example:

$$\Delta G_{mix} = \Omega_1 X_A X_B + RT(X_A \ln X_B + X_B \ln X_A) \quad (18)$$

For phase 1.

$$\Delta G_{mix} = \Omega_2 X_A X_B + RT(X_A \ln X_B + X_B \ln X_A) \quad (19)$$

For phase 2.

So:

$$b = X_A X_B \left[\frac{X_A \Omega_1 - X_B \Omega_2}{X_A - X_B} \right] + RT(X_A \ln X_B + X_B \ln X_A) \quad (20)$$

And m is:

$$m = \frac{X_A X_B (\Omega_2 - \Omega_1)}{X_B - X_A} \quad (21)$$

In equations (20) and (21), it is possible to appreciate that the change in the phases depends principally on Ω , and this is also $N_a z \epsilon$. Therefore, the mechanical properties of any material are easily transposable directly by the bond energy that exists between atoms.

When applying this method to a ternary alloy, the procedure is essentially the same, with the difference being that instead of having a tangent line, we have a tangent plane to the parabolas composed of each of the phases. **Figure 3** shows the formation of a ternary diagram from the curves of Gibbs free energy.

In the same fashion as the binary phase diagram, from the ternary diagram the percentage of each phase that exists for each composition can be obtained in such a way that it is possible to determine the mechanical, physical and chemical properties of each alloy. Therefore, it is possible — based on the composition and accordance with the phase diagram — to obtain the relationship with hardness. This is explained further in the next chapter.

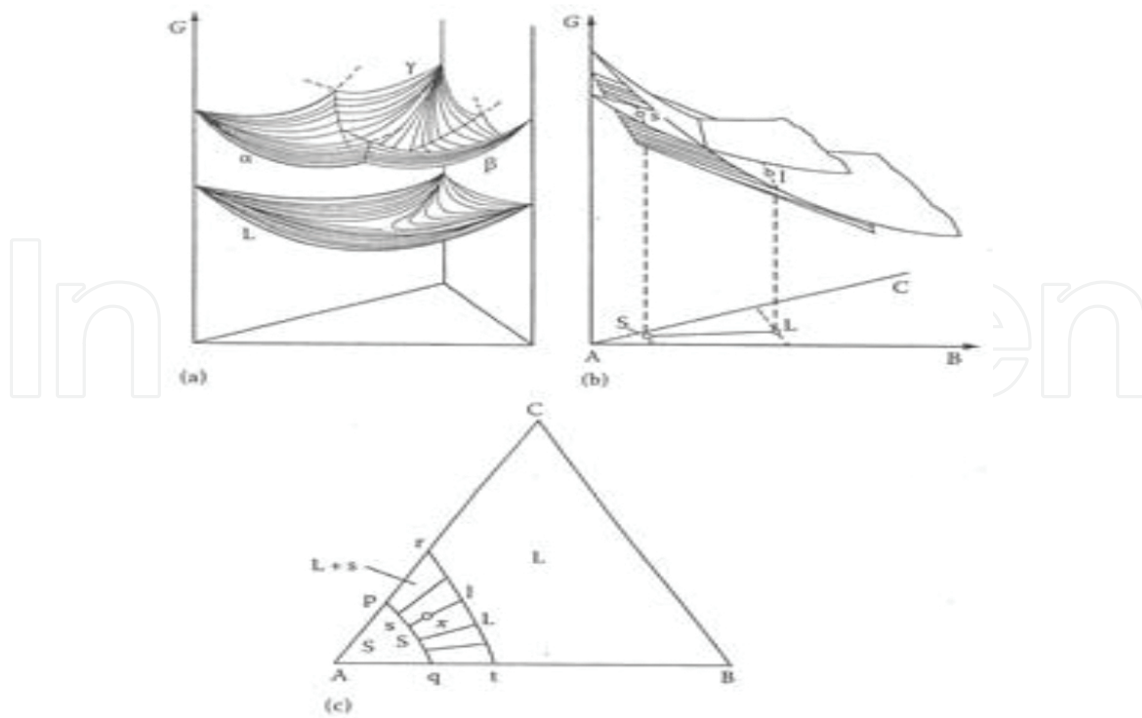


Figure 3. Representation of the ternary system curve developed with the Gibbs free energy [1].

3. Hardness

Hardness is defined as the capacity with which a body can contain the penetration of another body with a certain resistance. The deformation resistance is:

$$H = \frac{F}{A} \quad (22)$$

Where F is the force and A is the surface area.

The deformation of a sample during the indentation consist of two parts; the first part is elastic and the second is plastic.

Tabor's experimental studies suggest that hardness (H) is proportional to a representative tensile of contact σ_c ;

$$H = 2.7\sigma_c \dots \quad (23)$$

The answer of contact for materials of high hardness is often to the deformation elastic-plastic. These materials are governed by the equation:

$$\frac{H}{\sigma_r} = 1.44 + 0.264 \ln \left(\frac{E}{\sigma_r} \right) \quad (24)$$

where E is Young's modulus and equations (23) and (24) describe its relationship to the hardness. This is important because it is possible to obtain other mechanical properties only through the hardness.

In the last 10 years, new techniques have been developed in the measurement of hardness, such as micro and nanoindentation, in order to enable the complete characterization of mechanical properties in small areas the size of micrometers.

These techniques allow measurements of the curve force (P) and penetration (h). This curve describes the fundamental mechanical properties like Young's modulus and the stress-strain curve [3–7]. The micro and nanohardness allow for an assessment of the mechanical conduits to different levels microestructurales. The difference between macro, micro and nanoindentation is the load force. For example, in microhardness, the minimum load is 200 mN while in nanohardness it is 0.01 mN. The problem with micro and nanoindentation, is that they only can characterize an extremely small region of the sample, speak in clear of metallic materials.

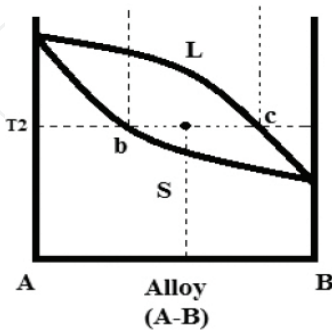
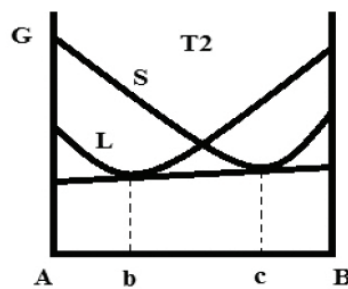


Figure 4. Alloy composed of L and S phases.

As previously mentioned, the points where a tangent line touches the two curves of the Gibbs free energy of each phase. **Figure 4** shows this:

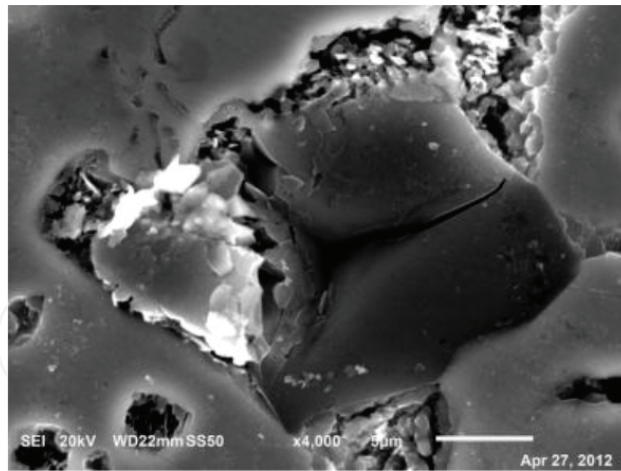


Figure 5. Nanoindentation seen by electronic microscopy.

The mechanical properties of any alloy are between point b and point c of **Figure 4**, and depend on the percentage of each phase present. For example, the alloy (a-B), consists of L and S phases, and to determine the percentage of each phase according to the chemical composition, it is necessary to use the lever rule. The alloy (A-B) can be measured with normal hardness and by the size of the track it generates, covering the two phases. As a result, the hardness is the average of the phases. However, when the hardness was measured with a nanohardness, only one phase was measured. For example, in **Figure 5** it is possible to appreciate the different phases present in the Al-Cu-Zn alloy. If we use conventional hardness, then the track is so big that it covers all the phases present, and nothing could observe the track to 4000 enhance.

The phase present in alloys, depends on temperature and pressure, and hence distinct phase diagrams can be seen according to these two variables.

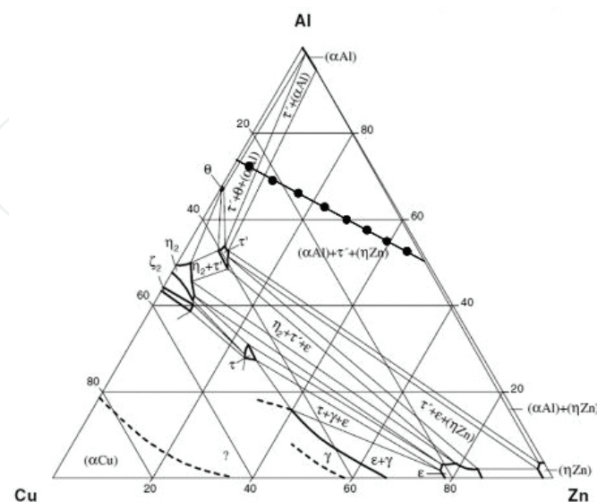


Figure 6. Ternary phase diagram of Al-Cu-Zn alloy. The line crosses the zone composed by the α , η and τ phases [8].

Figure 6 shows a ternary phase diagram of Al-Cu-Zn alloy to 200°C, at atmospheric pressure. A diagram of this kind does not exist in the literature at room temperature and all that's left is to think that keep the phases present of 200°C at room temperature. **Figure 6** shows a line that crosses the zone composed of the α , η γ and τ phases. Each point on this line is one alloy, with a different percentage chemical composition, and of phases, each of these alloys will have certain mechanical properties.

The line that crosses the diagram can be modelled by a linear equation in such a way that this equation will have a relationship with the mechanical properties of the alloy. It is possible to assess the mechanical properties of each of the alloys that are on the line. The next section describes the methodology of the assessment of hardness, and the analysis of phases.

4. Assessment of hardness for Al-Cu-Zn alloys in as-cast, homogeneized and quenching conditions

4.1. Introduction

"The Al-Zn-Cu ternary system is one of the most important alloy systems. It is important for the 7xxx series Al-based alloys and Zn-Al based alloys, ZAMAK. For instance, Zn-Al-Cu alloys have been used in different tribological applications as a substitute to conventional bearing bronzes and cast irons. Nevertheless, these alloys have some limitations such as dimensional stability because of the transformation of the metastable (CuZn_4) with a hexagonal crystalline structure into the stable τ' ($\text{Al}_4\text{Cu}_3\text{Zn}$) phase with an ordered rhombohedral structure. It is formed by the four phase reaction $\alpha + \varepsilon \rightarrow \eta + \tau'$ which also involves the fcc Al-rich α and cph Zn-rich η phases. The low tensile strength of these alloys at temperatures above room temperature has been attributed to their low melting points and they also have low ductility and high cracking tendency caused by the presence of the Zn-rich and Cu-rich phases. In order to overcome these limitations, the change in chemical composition has been proposed as an alternative. For instance, it has recently been proposed to change the base from zinc to aluminium. Replacing zinc with aluminium in the alloy system causes the formation of the stable θ (CuAl_2) with a tetragonal crystalline structure instead of the metastable ε phase, promoting a considerably higher ductility. Therefore, the purpose of this work was to investigate the effect of change in chemical composition on the microstructure, mechanical properties and hardness, in order to establish a relationship which enables us to assess the hardness in the as-cast and homogenized alloys" [9].

4.2. Methods and materials

Two lines of work were developed, composed of 8 samples of each line, as shown in **Figure 7**. For line 1, the samples M1 to M8 were developed and for line 2 the samples M9 to M16 were developed. **Table 1** shows the chemical composition of each of the samples.

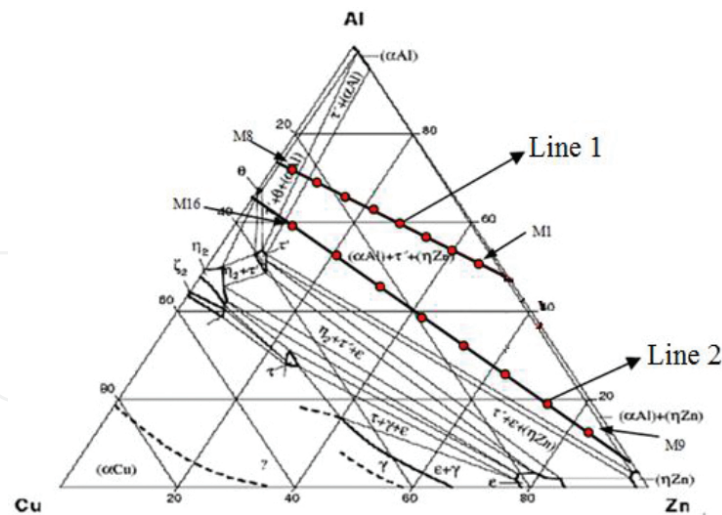


Figure 7. Ternary phase diagram of Al-Cu-Zn alloy, showing the two lines used. The points represent the alloys that were used in this work [8].

Every line is represented by an equation, so line one is represented by equation (25) and line two by equation (26).

$$X_{Zn1} = -1.9438(X_{Cu}) + 0.50334 \quad (25)$$

$$X_{Zn2} = -2.9823(X_{Cu}) + 0.97337 \quad (26)$$

where X_{Zn} and X_{Cu} are the atomic fractions of Zn and Cu respectively. The rest is Al, completing the 100%.

Sample	Cu		Zn		Al		Sample	Cu		Zn		Al	
	%p.	%at.	%p.	%at.	%p.	%at.		%p.	%at.	%p.	%at.	%p.	%at.
M1	5.00	3.54	63.18	43.44	31.82	53.02	M9	5.00	4.77	89.60	83.10	5.4	12.13
M2	10.00	6.87	55.31	36.96	34.70	56.17	M10	10.00	9.02	80.32	70.42	9.68	20.56
M3	15.00	10.03	47.43	30.82	37.57	59.15	M11	15.00	12.83	71.04	59.05	13.96	28.12
M4	20.00	13.01	39.56	25.02	40.44	61.97	M12	20.00	16.26	61.76	48.81	18.24	34.93
M5	25.00	15.84	31.69	19.52	43.31	64.64	M13	25.00	19.37	52.48	39.52	22.52	41.01
M6	30.00	18.53	23.82	14.30	46.19	67.17	M14	30.00	22.20	43.19	31.07	26.81	46.72
M7	35.00	21.08	15.94	9.33	49.06	69.59	M15	35.00	24.79	33.91	23.35	31.09	51.86
M8	40.00	23.51	8.07	4.61	51.93	71.88	M16	40.00	27.17	24.63	16.26	35.37	56.57

Table 1. Chemical percentage of each sample.

Each sample was prepared by the melting of pure elements at 750 °C under an argon atmosphere and then slow cooling. Alloys were homogenized at 350 °C for 180 h in order to eliminate the dendritic structure. All alloys were subsequently heated to 350 °C for 24 h and quenched

Fases	Temperature (°C)	Muestra	Fases	Temperature (°C)	Muestra
τ, α	400	M1 – M6	L, η	400	M9
θ, α, τ	400	M7 – M8	L, α, η	400	M10
			τ, α, η	400	M11 – M12
			θ, α, τ	400	M13 – M16
τ, α, α'	350	M1 a M4	α, η	350	M9
τ, α	350	M5- M7	τ, α, η	350	M10 – M11
τ, α, θ	350	M8	τ, α	350	M12 – M14
			τ, α, α'	350	M15
			τ, α	350	M16
τ, α, α'	300	M1 – M5	τ, α, η	300	M9 – M12
τ, α	300	M6 – M7	τ, α	300	M13
τ, α, θ	300	M8	τ, α, α'	300	M14 – M16
τ, α, η	25	M1 – M7	τ, α, η	25	M9 – M16
τ, α, θ	25	M8			

Table 2. Phases present in each sample at specific temperatures according to Thermo-Calc.

Samples M1 to M8 show many changes in phase between 20 °C to 300 °C, compared to samples M10 and M11. Therefore, and as can be seen in the hardness results, samples M1 to M8 have an increase in the hardness of heat treatment to other.

The Thermo-Calc program also shows that the Börnstein's diagram is perfectly in line with these observations.

4.3.2. Structural and microstructural characterization of the alloys

The diffraction patterns of samples M1 to M8, and M9 to M16 are presented in **Figures 9** and **10** respectively.

Figure 10 shows that α, η, ϵ and τ phases are present in nearly all as-cast alloys. "The increase in Cu content was observed to be related to the increase in the intensity of X-ray diffraction peaks corresponding to the θ phase. This phase may be formed by the eutectic reaction $L \rightarrow \alpha + \theta$ located in the Al-Cu rich side. In contrast, the peak intensity of the Zn-rich η phase also increases with an increase in Zn content. This fact suggests the increase in the volume fraction of this phase. The amount of α and ϵ phases showed no clear tendency to increase or decrease the contents of either Al or Zn. A low volume fraction of the β phase is present in the as-cast M1 to M7, M9, and M14 to M16 alloys. This presence seems to indicate that the chemical compositions of alloys on line 1 are closer to the β phase field at high temperatures than the alloy compositions on line 2. Likewise, the τ' phase is, in general, more stable as the Cu content increases. This suggests that the four-phase reaction, $\alpha + \epsilon \rightarrow \eta + \tau'$, took place during the cooling of these alloy compositions"[11].

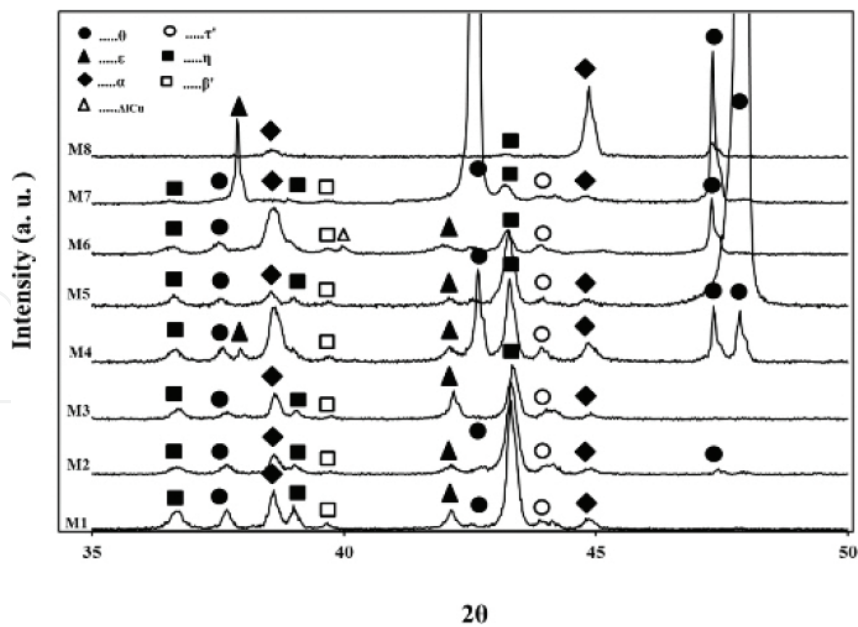


Figure 9. Diffraction pattern in as-cast alloys of samples M1 to M8.

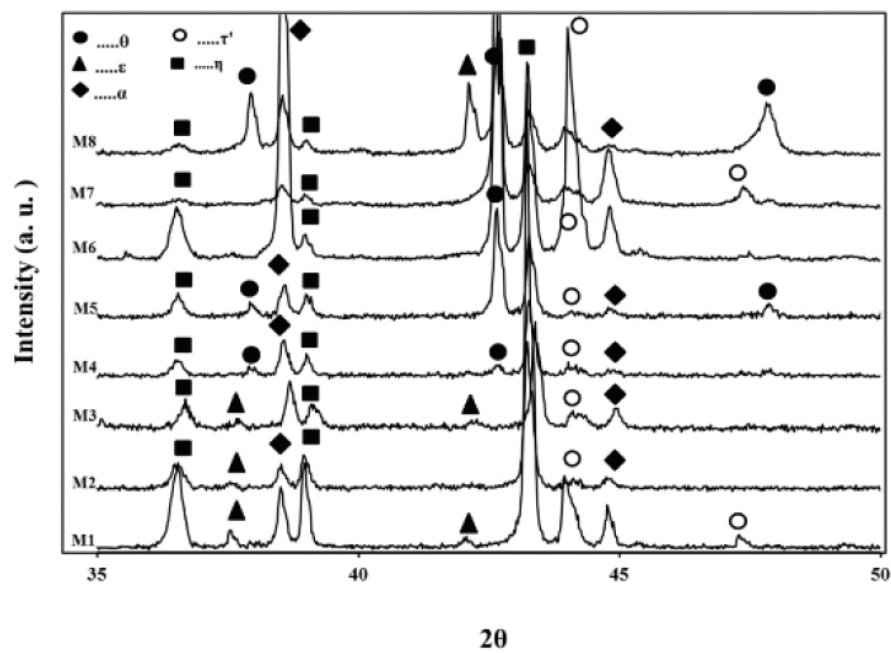


Figure 10. Diffraction pattern in as-cast alloys of samples M9 to M16.

Micrographs taken by SEM of samples M2, M7, M10 and M15 are shown in **Figure 11**.

The micrographs show that there is an increase in the percentage by volume of the θ phase with respect to an increase in the quantity of Cu and Al. All samples with a low Cu and Al content show a very heterogeneous microstructure, while samples with a high content of these elements show a uniform appearance.

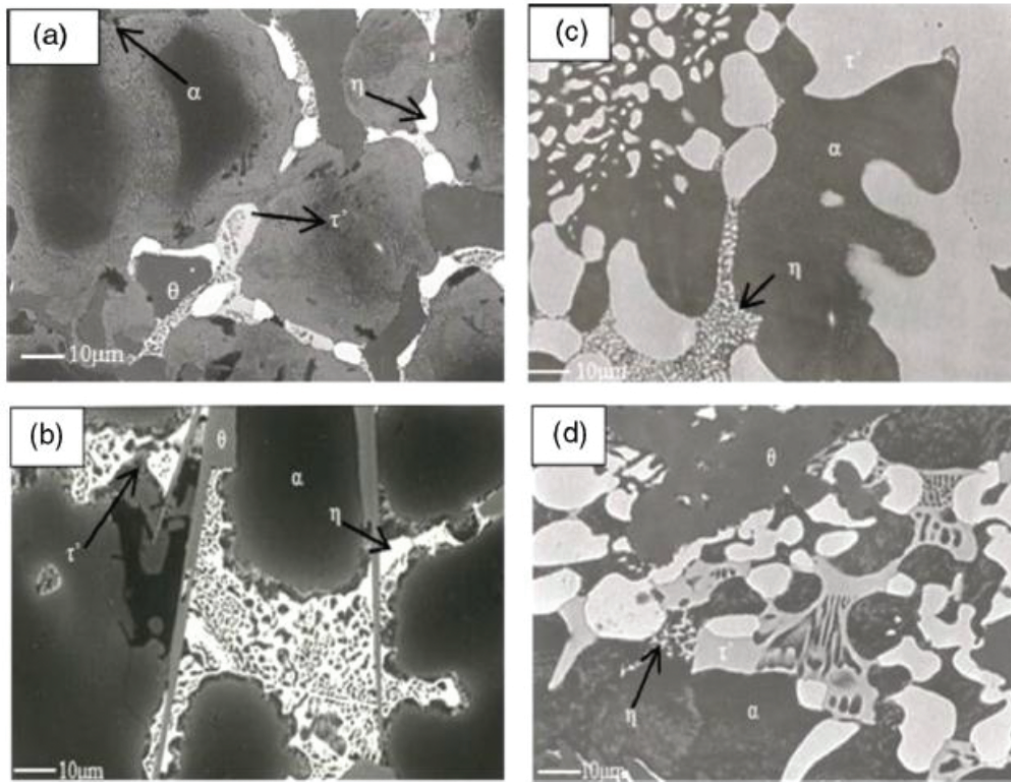


Figure 11. SEM Micrographs of different as-cast samples, (a) sample M2, (b) sample M7, (c) sample M10 and (d) sample M15.

Figures 12 and 13 show the diffraction patterns of the homogenized samples M1 to M16.

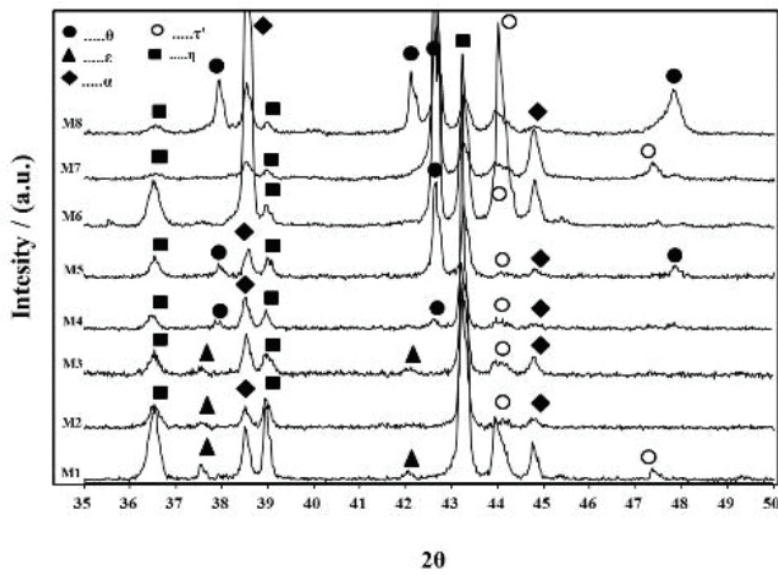


Figure 12. Diffraction pattern of the homogenized samples M1 to M8.

The ε phase appears in samples M1 to M3. This is important because the phase is present in the transformations of the four phases. Samples M4 to M8 do not have the ε phase, but they have the θ phase, which is more stable because it is not involved in the transformation of the four phases [12]. In the samples of series two, the ε phase is presented in samples M9 to M13, and the θ phase in samples M15 to M16 even though it should be emphasized that in these samples the β phase is present. It should be remembered that the β phase, in accordance with Aragon's investigations [13] occurs after quenching and then disappears after this to room temperature when Cu is present in small proportions. However, when the content of Cu is enhanced, the β phase is retained and is harder to eliminate.

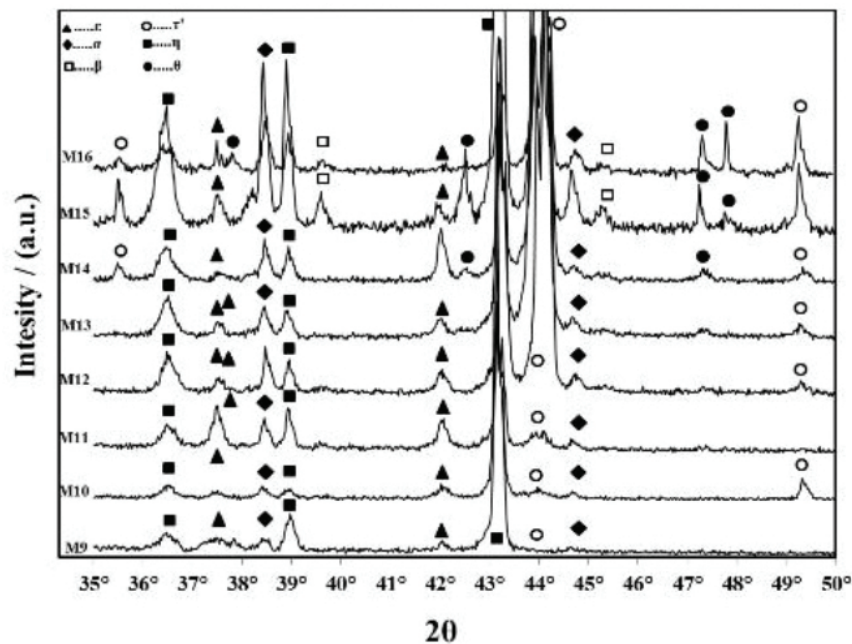


Figure 13. Diffraction pattern of the homogenized samples M9 to M16.

It can also be observed that an enhanced volumetric of the θ phase causes an increase in the hardness of the samples.

Figure 14 (a) and (b) show the diffraction patterns after quenching. Samples M1 to M4, and M9 to M11 show the same phases as follow the process of homogenization. However, when comparing the diffraction patterns of homogenized and quenching alloys of these samples, an increase in the intensity of both τ and α phases can be observed. It should be noted that the samples are solid and not in powder form, therefore there is texture, but even so it is possible to observe an increase in the phases.

Figure 15 shows micrographs of samples M2 (a–b) after homogenized, and sample M8 (c–d) after quenching. We can see that in sample M2 there is no dendritic structure. Moreover, when we compare samples M2 and M8, it can be seen that an increase in the quantity of Al and Cu enhances the percentage of the θ phase.

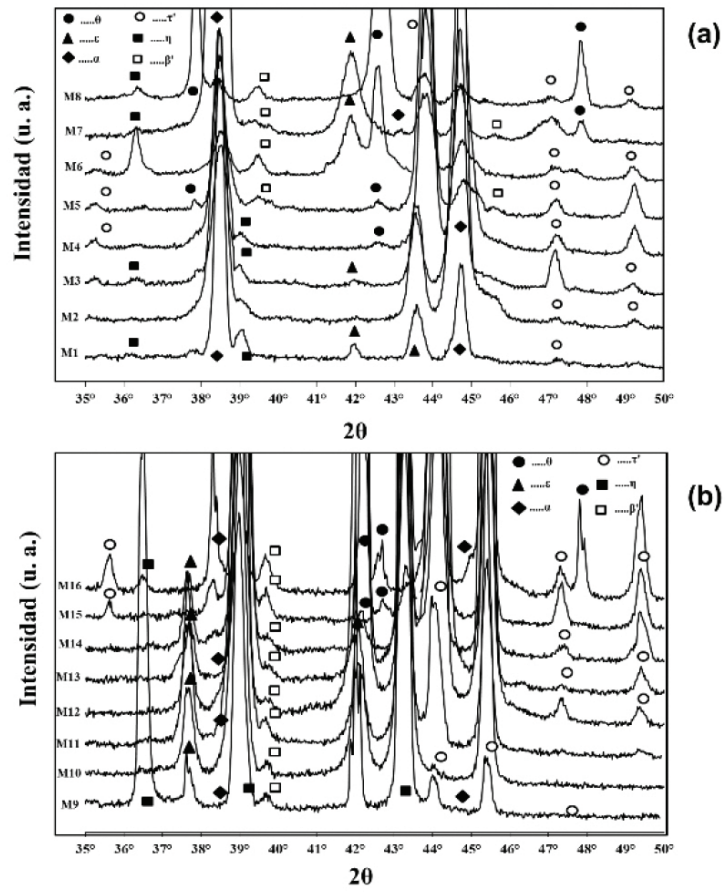


Figure 14. Diffraction patterns of samples M1 to M16 after quenching: (a) samples M1 to M8, (b) samples M9 to M16.

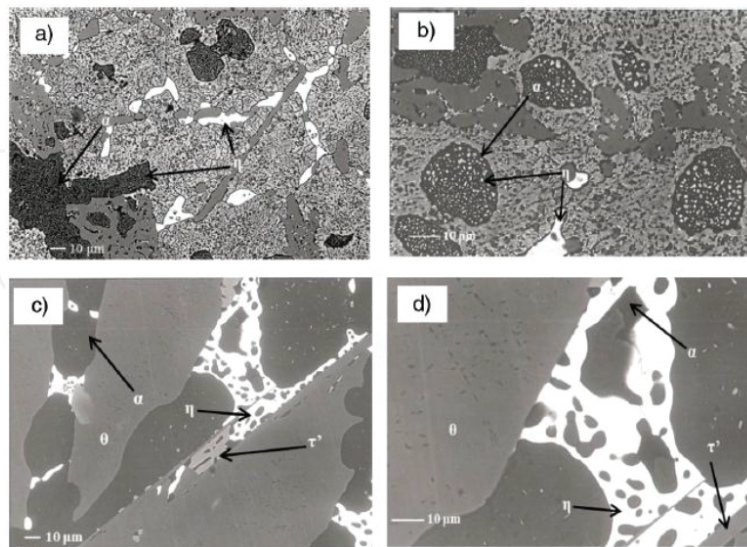


Figure 15. Micrographs of samples M2 and M8: (a) Sample M2 homogenized to 400X, (b) Sample M2 homogenized to 1000X, (c) Sample M8 quenching to 400X, (d) Sample M8 quenching to 1000X.

5. Hardness results

The hardness obtained from each of the samples, namely as-cast, homogenized and quenching, is shown in **Figure 16**. Each thermal process of the series 1 compound for samples M1 to M8, as well as the series 2 compound for samples M9 to M16, shows a linear trend.

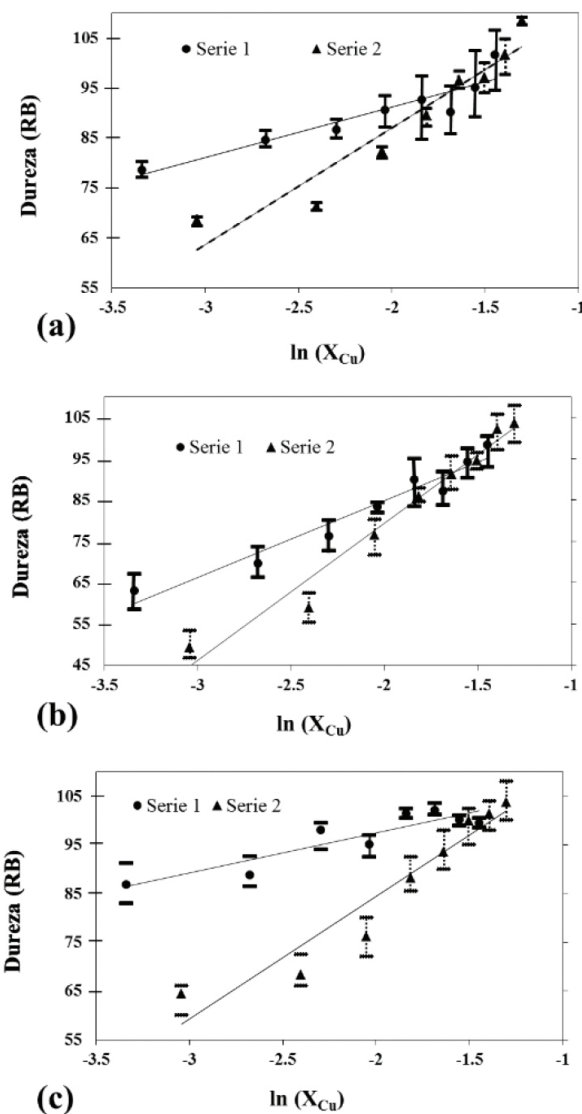


Figure 16. Graphic of the hardness of samples M1 to M16 subjected to different heat treatments, (a) as-cast; (b) homogenized and (c) quenching [10].

Using a least squares regression produces a correlation coefficient of between 0.82 and 0.97, indicating a good fit. The table shows the equations that relate the hardness to the chemical composition of each of the samples.

The equations in **Table 3** are used in order to provide an assessment of hardness according to chemical composition. In these equations, the value of only one of the three elements used in

the alloy is present. As a result, it is necessary to use equations 27 and 28. If a certain hardness is desired in accordance to a certain heat treatment, then we use the equation relating to that heat treatment. For example, if you want to have 65 RB after a homogenized heat treatment, then the homogenized equation of **Table 3** should be used, but the series 1 and 2:

$$63 = 18.617 \ln X_{Cu} + 122.12 \quad \dots \text{series 1}$$

$$63 = 33.326 \ln X_{Cu} + 146.05 \quad \dots \text{series 2}$$

Treatment Thermic	Equation	R ²
Series 1		
As-Casting	HB = 10.12 lnX _{Cu} + 111.38	0.8673
Homogenizad	HB = 18.617 lnX _{Cu} + 122.12	0.9464
Quenching	HB = 8.1666 lnX _{Cu} + 113.81	0.8197
Series 2		
As-Casting	HB = 23.334 lnX _{Cu} + 133.63	0.9169
Homogenizad	HB = 33.326 lnX _{Cu} + 146.05	0.9704
Quenching	HB = 25.211 lnX _{Cu} + 134.83	0.9186

Table 3. Equations generated from linearly regressing each heat treatment with respective values of R².

To resolve X_{Cu}:

$$X_{Cu} = 0.04204 \quad \dots \text{atomic fraction of series 1}$$

$$X_{Cu} = 0.08274 \quad \dots \text{atomic fraction of series 2}$$

In order to know the atomic fractions of Zn and Al, equations (25) and (26) are used,

$$X_{Zu1} = -1.9438(0.04204) + 0.50334 = 0.4216 \quad \dots \text{atomic fraction of Zn series 1}$$

$$X_{Zu2} = -2.9823(0.08274) + 0.97337 = 0.7266 \quad \dots \text{atomic fraction of Zn series 2}$$

Therefore, in order to have an alloy with 63 RB, it is necessary to have 4.204 % at. Cu, 42.16% at. Zn and 56.63% of Al in the case of series 1.

However, it is also possible to obtain 63 RB by using 8.27% at. Cu, 72.66% at. Zn and 19.06% at. Al.

As can be seen, it is possible to obtain the same hardness, but with a different chemical composition. If we want to use less of the more expensive Cu, then there is a need to use an increased amount of Al, whereby we can have a product with the same mechanical properties

but at a cheaper cost. For example, the international standard cost of Aluminum is 1.55 dollars/kg, the cost of Cu is 8.2 dollar/kg and that of Zn 2.07 dollars/kg. If we require an amount of 100 kg of the product, then the cost will be of 247.86 dollars using a larger quantity of Cu. If the same product is made but a larger quantity of Al and Zn is used, then the cost is 204.82 dollars, making a saving of 17.36% —almost a fifth of the total product.

6. Assessment of hardness

Using the equations it is possible to produce an assessment of the hardness of any alloy that is found in the line of either series 1 or 2. However, it is also possible to produce an assessment of the hardness of any alloy which is situated between the two series. It must be remembered that equations (25) and (26) provide the chemical composition of any alloys that are on either line. The difference between the lines of series 1 or 2 is the angle, and this is directly proportional to the slope of the hardness. For this reason, it is possible to relate the two. **Figure 17**

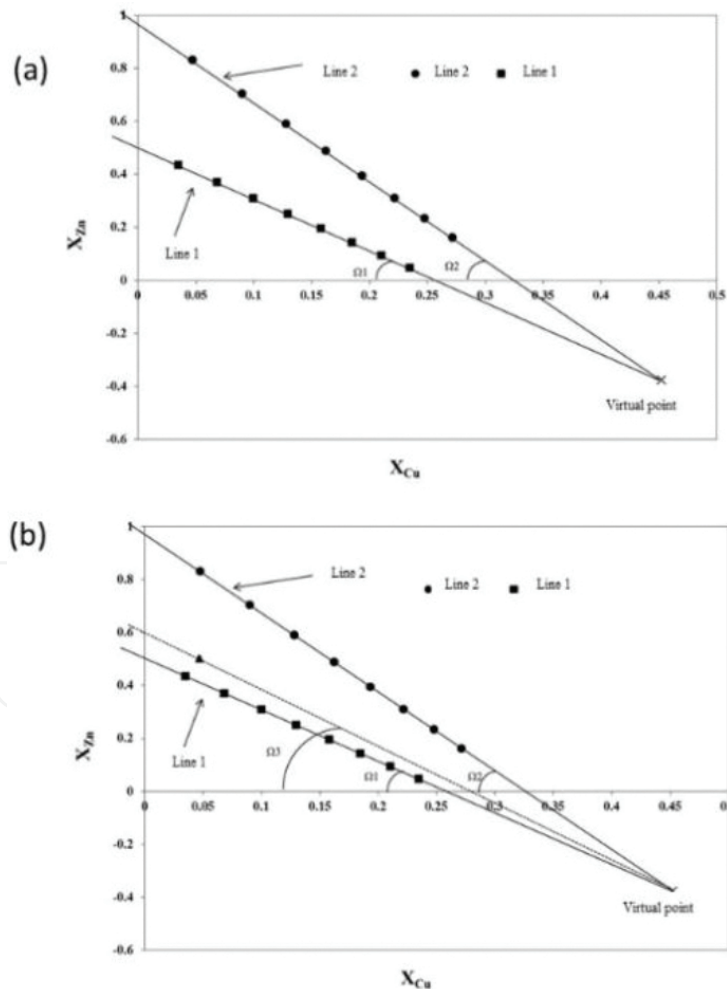


Figure 17. (a) Representation in cartesian coordinate of equations (27) and (28), (b) Representation of cartesian coordinate ZnAl₂₇Cu₃ [10].

shows a cartesian coordinate where “x” is X_{Cu} (the atomic fraction of Cu) and “y” is X_{Zn} (the atomic fraction of Zn) and the angle is represented by Ω_1 and Ω_2 .

In order to determine the angle, it is necessary to use a virtual point that is the intersection of the two lines in **Figure 7**, or of equations (25) and (26). This point is virtual because the percentage of Zn is negative (-37.46 % at.), and for this reason it is impossible for this point to exist. However, the virtual point is useful in determining the angle of any alloy that exists between these two lines.

For example, we can consider the alloy ZnAl27Cu3, which has 50.54% at. Zn; 2.23% at. Cu with the remaining percentage being Al [14]. The composition of ZnAl27Cu3 is only a point in the Cartesian coordinate and this point exists between line 1 and 2. When this point is joined with the virtual point, there is an angle of 63.99° as seen in **Figure 17(b)**. As mentioned above, there is a direct relationship between the slopes, composition and hardness. This is because the percentage of each of the phases changes with the chemical composition. Therefore it is necessary to elucidate the relationship between the angle in the Cartesian coordinate in the chemical composition (**Figure 17**), and the angle in the graphic of the hardness vs $\ln X_{Cu}$. For example, the angle of line 1 in the cartesian coordinate of the composition has a value of 62.78°, but the angle in the hardness in as-cast, is 84.74° and the same occurs with line 2. In the case of the alloy ZnAl27Cu3, the angle of hardness is found by interpolation, as seen in **Table 4**.

Sample	Angle (Percentage at. of each element)	Angle (Hardness in as-cast)
Line 1	62.78°	84.74°
ZnAl27Cu3	63.99°	85.13° by interpolation
Line 2	71.47°	87.55°

Table 4. Results of the angles of each of the series according to its composition and hardness in as-cast.

Once the slope of hardness in the ZnAl27Cu3 alloy is present, the hardness intercept is then required. For this, is necessary to first obtain the hardness equation and then subsequently the hardness of the alloy according to the chemical composition. The intercept of the origin is obtained using the point of interception that exists between the equations of hardness. For example, the point of intersection in the equations in as-cast is 18.57% at. Cu and 94.34 RB. The point of intersection is shown in **Figure 16(a)**.

At this point, we have the slope, the hardness and the percentage Cu, therefore the equation is:

$$94.34 = \tan(85.13)\ln(0.1857) + b$$

Solve for b

$$b = 94.34 - \tan(85.13)\ln(0.1857) = 114.11$$

So the equations of the line that crosses for the ZnAl27Cu3 alloy is:

$$HB = \tan(85.13) \ln(X_{Cu}) + 114.11$$

If the atomic percentage of ZnAl27Cu3 alloy is 50.54% at. Zn; 2.23 % at. Cu and the remaining percentage being Al then the hardness is:

$$HB = \tan(85.13) \ln(0.023) + 114.11 = 69.45$$

The result obtained by Savaskan [14] was 67.15 RB with an error of only 5.43%. In this way, any alloy between the two lines can be assessed, as long as it has a heat treatment of as-cast, homogenized or quenching.

Tables 5 and **6** show the assessment obtained by this method for certain alloys made by Savaskan and Ciach [14, 15].

Sample	Savaskan et al. (2003)	Assessment	Error (%)
ZnAl27Cu1	64.74	59.94	7.41
ZnAl27Cu2	66.21	66.98	1.15
ZnAl27Cu3	67.15	71.04	5.48
ZnAl27Cu4	68.5	73.91	7.32
ZnAl27Cu5	70.75	76.12	7.05
		Error average =	5.68

Table 5. Comparative results of hardness as determined by Savaskan et al. (2003) and the assessment values.

Sample	Savaskan et al., (2003)	Assessment	Error (%)
AlZn78Cu1	73	66.99	7.41
AlZn78Cu2	78	73.12	1.15
AlZn78Cu3	81	76.53	5.48
		Error average =	6.67

Table 6. Comparative results of hardness as determined by Ciach et al. (1969) and the assessment values.

The same methodology can be used in any ternary alloy as long as there is a phase diagram, and this methodology can even be used with commercial alloys and the average error is only 5%. Therefore, it is possible to obtain alloys tailored to any ternary alloy, or to develop alloys cheaper or with better mechanical properties.

7. Conclusions

- The evidence from equations (20) and (21) shows a direct relationship between the bond energies of the atoms (Ω) and the mechanical properties in such a way that in future it will be possible to directly obtain the mechanical properties of bond energies.
- The θ phase increases the hardness, and this phase intensifies along with an increase of Al and Cu.
- The β phase along with ϵ phase causes a decrease in hardness.
- The β phase remains to room temperature with an increase of Cu.
- The simulation using Thermo-Calc enables a better understanding of the changes of phase shown in each of the samples.
- The methodology presented here has been shown to be very effective, and it is possible use this methodology with other alloys.
- It has also been shown that is possible to obtain alloys with similar mechanical properties, but at a cheaper cost.

Author details

Jose David Villegas Cárdenas^{1*}, Victor Manuel López Hirata², Carlos Camacho Olguin¹, Maribel L. Saucedo Muñoz² and Antonio de Ita de la Torre³

*Address all correspondence to: jdvc76@yahoo.com.mx

1 Universidad Politécnica del Valle de México

2 Instituto Politécnico Nacional

3 Universidad Autónoma Metropolitana

References

- [1] Porter, D., Easterling, K., Sherif, M., (2009) "Phase transformations in metals and alloys", Ed. CRC Press, 3er edic. E.U., 1 – 105.
- [2] Konrad, H. (2011), "Harness testing: principles and applications", Ed. ASM international, isbn 1615038329, 978-1-61503-832-9, 1er edic, E.U. 50 – 250.

- [3] Alcalá, J., Giannakopoulos, A. E., & Suresh, S. (1998). Continuous measurements of load-penetration curves with spherical microindenters and the estimation of mechanical properties. *Journal of Materials Research*, 13(05), 1390-1400. 1997.
- [4] Alcalá, J., (2000), "Instrumented micro-indentation of zirconia ceramics", *J. Am. Ceram. Soc.*, No. 83, p. 1977-1984.
- [5] Suresh, S. Giannakopoulos, A., Alcalá, J. (1997), "Spherical indentation of compositionally graded materials: theory and experiments", *Acta Mater.*, No. 45, p. 1307-1321.
- [6] Alcalá, J., Gaudette, F., Suresh, S., Sampath, S., (2001) "Instrumented spherical micro-indentation of plasma-sprayed coatings", *Mater. Sci. & Engrn. A*, No. 316, p. 1-10.
- [7] Dao, M., Chollacoop, N., Van Vliet, K., Venkatesh T., Suresh, S., (2001) "Computational modeling of the forward and reverse problems in instrumented sharp indentation", *Acta Mater.*, No. 49, p. 3899-3918.
- [8] Bornstein, L. (2005). Ternary Alloy System Phase Diagrams, Crystallographic and Thermodynamic Data, Ed. Springer, Vol. 1, 11, New York, USA, pp. 183–205.
- [9] Villegas-Cardenas, J. D., Lopez-Hirata, V. M., Torre, A. D. I. D. L., & Saucedo-Munoz, M. L. (2011). Assessment of hardness in as-cast and homogenized Zn-Al-Cu alloys. *Materials Transactions*, 52(8), 1581-1584.
- [10] Villegas J. D., Saucedo M. L., Lopez V. M., Dorantes H. J., "Predicción de la dureza de aleaciones Al-Cu-Zn en estado de colada y templado", *Revista de Metalurgia*, Vol. 50, No. 2, 2014. DOI: 10.3989/revmetalm.015
- [11] Villegas J. D., Saucedo M. L., Lopez V. M., Dorantes H. J., "Effect of phase transformations on hardness in Zn-Al-Cu alloys". *Materials Research*, V17, No. 5. DOI:<http://dx.doi.org/10.1590/1516-1439.228913>.
- [12] Savaskan, T., Heikimoğlu, P., PURcek, G. (2004). Effect of copper content on the mechanical and sliding wear properties of monotectoid-based zinc-aluminium-copper alloys. *Tribol. Int.* 37 (1), 45–50. [http://dx.doi.org/10.1016/S0301-679X\(03\)00113-0](http://dx.doi.org/10.1016/S0301-679X(03)00113-0).
- [13] Aragon, J.A., Miranda, J.R., Garcia, A. (2007b). Obtencion de una microestructura nueva en la aleacion Zn -40% at. Al-1,5 % at. Cu. *Rev. Mex. Fís.* 53 (3), 149–158. http://rmf.smf.mx/pdf/rmf/53/3/53_3_149.pdf.
- [14] Savaskan, T., Purcek, G., Heikimoğlu, P. (2003). Effect of copper on the mechanical and tribological properties of ZnAl27 based alloys. *Tribol. Lett.* 15 (3), 257–263.<http://dx.doi.org/10.1023/A:1024817304351>.
- [15] Ciach, R., Krol, J., Wegryn, K. (1969). Studies on four phases transformation in AlZn78 alloy containing 1–3 per cent of copper. *Bulletin de L'Academie Polonaise des Sciences* 17 (4), 371–378.

